RSC Advances

PAPER

View Article Online
View Journal | View Issue

Cite this: *RSC Adv.*, 2019, **9**, 22772

Top-down synthesis of sponge-like Mn_3O_4 at low temperature†

Wangwei Lu,[a] Kay He,[a] Gaoling Zhao,[a]* Bin Song,[b] Jing Zhou,[ac] Weixia Dong[ad] and Gaorong Han[a]

A top-down synthetic method was developed for the fabrication of sponge-like Mn_3O_4 composed of Mn_3O_4 nanocrystals by decomposition of manganese formate at 200 °C. The samples were characterized in terms of their structural and morphological properties by means of X-ray diffraction (XRD), scanning electron microscopy (SEM), transmission electron microscopy (TEM) and Brunauer–Emmett–Teller (BET) studies. TEM and SEM images showed that the morphology of sponge-like Mn_3O_4 structures was mostly retained from the morphology of the manganese formate precursor, which was controlled by the solvothermal process. Large sponge-like Mn_3O_4 structures exhibiting crystallographic symmetry were prepared under solvothermal treatment for a long time. The XRD pattern showed that the Mn_3O_4 exhibit a tetragonal hausmannite structure. The results of N_2 adsorption analysis indicated that the sponge-like Mn_3O_4 nanostructures possess high surface area. The possible formation mechanism of Mn_3O_4 nanostructures has been discussed.

Received 23rd May 2019
Accepted 10th July 2019

DOI: 10.1039/c9ra03893k

rsc.li/rsc-advances

1. Introduction

Manganese oxides, both amorphous and crystalline, have attracted great attention because of their abundant properties caused by multi-valence. For example, amorphous manganese oxides provided the highest turnover numbers as water oxidation catalysts.[1] On the other hand, Mn_3O_4 (hausmannite) has been studied due to its promising application in fields such as rechargeable lithium ion batteries,[2–4] supercapacitors[5–8] and active catalysts for the oxidation of NO_x and carbon monoxide.[9,10] It is also a starting material for manufacturing manganese zinc ferrite used as soft magnetic materials and lithium manganese oxides used as electrode materials due to its low cost and great environmental compatibility. Considerable interest has been paid to synthesizing Mn_3O_4 nanostructures,[11,12] for instance, nanoparticles,[13–16] nanorods,[17,18] nanowires or nanofibers,[19,20] nanoplates,[21] superlattices[22] and hierarchical nanostructures.[23–28] Among these, hierarchical Mn_3O_4 nanostructures take advantage of both nanometer-sized building blocks and micro-sized assemblies. Hierarchical Mn_3O_4 nanostructures with remarkably increased surface areas are expected to display better performance in applications as rechargeable lithium ion batteries, supercapacitors and active catalysts.

The existing methods to fabricate hierarchical structures can be generally classified as bottom-up or top-down approaches. The bottom-up approach, which has been extensively researched over the past decade, assembles the nanometer-sized building blocks to hierarchical structures with the help of structural directing agents.[23,25,26] However, the bottom-up approach may be quite complex and the controlled-synthesis of hierarchical structures may be difficult. On the other hand, top-down fabrication offers a greater flexibility and controllability, and it is much more suitable for the production of hierarchical structures.[29] Recently, the nanostructures, such as Fe_3O_4,[30] ZnO,[31] Co_3O_4,[32] In_2O_3 [33] or carbon,[34] are fabricated *via* top-down strategy using various preformed MOFs (Metal–Organic Frameworks) as precursor. Due to the high content of organic matters in the MOFs, if great structural collapse is avoid, the inorganic frameworks with a large number of pores can be obtained by removing the organic matters after the heat treatment. However, high temperature (450–1000 °C), aimed to remove the organic matters and form crystals, is needed because of the high thermal stability of the MOFs. In this circumstance, it is difficult to avoid the collapse or deformation of the structures. In order to reduce the heat treatment temperature, it is preferred to use the MOFs with low decomposition temperature. Manganese formate is one of MOFs that have the simple topology and the low molecular weight, which

[a]*State Key Laboratory of Silicon Materials & School of Materials Science and Engineering, Zhejiang University, Hangzhou 310027, P. R. China. E-mail: glzhao@zju.edu.cn*

[b]*State Key Laboratory of Silicon Materials & Department of Physics, Zhejiang University, Hangzhou 310027, P. R. China*

[c]*Department of Forensic Science, Zhejiang Police College, Hangzhou 310053, P. R. China*

[d]*School of Materials Science and Engineering, Jingdezhen Ceramic Institute, Jingdezhen, Jiangxi 333403, P. R. China*

† Electronic supplementary information (ESI) available. See DOI: 10.1039/c9ra03893k

are suggested to have low decomposition temperature. Even so, the decomposition of manganese formate starts at 350 °C detected by thermal analysis under N_2 atmosphere.[35] Based on these perspectives, hierarchical Mn_3O_4 nanostructures with remarkably increased surface area are expected to be prepared at low temperature.

Herein, in order to study a low temperature way to obtain high surface area Mn_3O_4, a facile top-down method was developed to prepare hierarchical sponge-like Mn_3O_4, starting from manganese formate. The manganese formate was prepared by precipitation at room temperature using manganese(II) acetate tetrahydrate as a Mn source. Effects of the preparation parameters, such as the heat treatment temperature, the concentration of formic acid and the solvothermal time, on the morphology and crystallinity were investigated. The formation mechanism of the sponge-like Mn_3O_4 structures was proposed. The surface area of the samples were also investigated.

2. Experiment

2.1. Preparation

All the regents were used as received without further purification. In a typical procedure, 1.1 g manganese(II) acetate tetrahydrate was dissolved in anhydrous ethanol (30 mL) to get a transparent solution. Some amount of formic acid was mixed with the solution and white precipitation was instantly appeared. Parts of the suspension were centrifuged, washed with ethanol several times, dried in air at 80 °C, and finally placed into a muffle furnace at 200 or 350 °C for 12 h. The solid products before heat treatment and after heat treatment were both collected for characterization. The solvothermal process was employed to grow manganese formate before the heat treatment. The suspension was sealed within a Teflon-lined autoclave (40 mL) which was filled about 80% of its capacity and heated at 150 °C under a solvothermal condition for various time. The solid products were collected by centrifugation, washed with ethanol several times, dried in air at 80 °C, and finally placed into a muffle furnace at 200 °C for 12 h.

2.2. Characterization

Powder X-ray diffraction (XRD) was used to characterize phase and crystallinity of the samples. Data were collected on a X'Pert PRO X-ray diffractometer with Cu Kα radiation ($\lambda = 1.54178$ Å) at a beam current of 40 mA. The morphologies of the samples were investigated using a Hitachi S-4800 field-emission scanning electron microscope (FE-SEM) with cold field emitter. Energy dispersive X-ray analysis (EDX) was carried out on a Hitachi S-4800 with the attachment. Transmission electron microscopy (TEM) was used to observe the morphology and investigate the crystallographic characteristics of the samples. TEM studies were carried out on a Tecnai F20 with accelerating voltage of 200 kV. The thermogravimetric analysis was performed on a TA-Q500 (TA Instruments) with a heating rate of 10 °C min^{-1} in air. The differential thermal analysis was performed on a CRY-2 analyzer with a heating rate of 10 °C min^{-1} in air. The Brunauer–Emmett–Teller (BET) surface area was measured by a gas adsorption apparatus (AUTOSORB-1-C).

3. Results and discussion

3.1. Effects of heat treatment on the morphology and crystal phase of Mn_3O_4

Fig. 1 shows XRD patterns of the samples prepared with 0.68 M formic acid before heat treatment and after heat treatment at 200 °C, as well as XRD calculation pattern of manganese formate. The crystal structure of manganese formate for the calculation is obtained from Dybtsev.[35] According to XRD calculation pattern of manganese formate (see the curve a of Fig. 1), the diffraction peaks of the sample prepared with 0.68 M formic acid before heat treatment (see the curve b of Fig. 1) are indexed to manganese formate. The diffraction peaks of the sample prepared with 0.68 M formic acid after heat treatment at 200 °C (see the curve c of Fig. 1) are indexed to hausmannite (JCPDS no. 80-0382). Hausmannite is a prototype of the spinel structure with lattice parameters $a = b = 5.762$ Å and $c = 9.4696$ Å and space group $I4_1/amd$ (no. 141).

Fig. 2 shows thermogravimetric analysis of manganese formate prepared with 0.68 M formic acid. The decomposition of manganese formate can be divided into two stages. The first stage of weight loss occurs around 180 °C, corresponding to the loss of guest molecules in the channels, including water, oxygen, *etc.*[36] In the first stage, the weight loss is about 3.6%. The second stage occurs from 200 °C to 268 °C. In the second stage, the weight loss is 44.9%. In view of the molecular weight of manganese formate and hausmannite is 145.0 g mol^{-1} and 228.8 g mol^{-1}, respectively. Thus, the weight loss during the decomposition of manganese formate is 47.4% in theory, which is close to the weight loss in second stage. Accordingly, in the second stage the process accounting for this significant weight loss can be ascribed to decomposition of manganese formate. Most of the weight loss occurs between 258 °C and 268 °C,

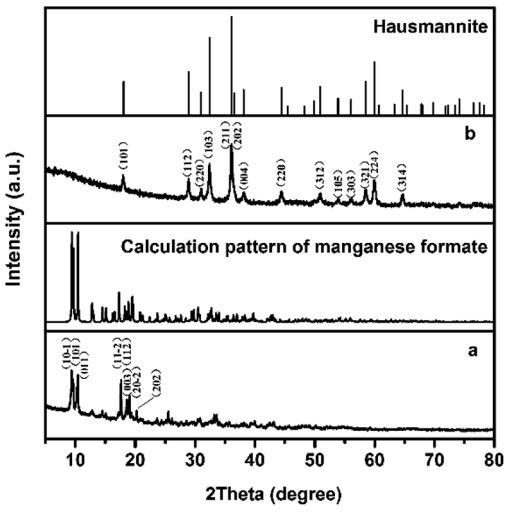

Fig. 1 XRD patterns of the samples prepared with 0.68 M formic acid (a) before heat treatment and (b) after heat treatment at 200 °C.

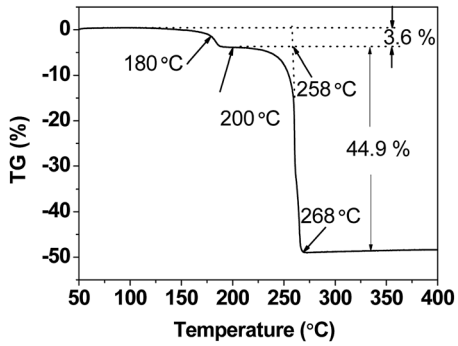

Fig. 2 Thermogravimetric analysis of manganese formate prepared with 0.68 M formic acid.

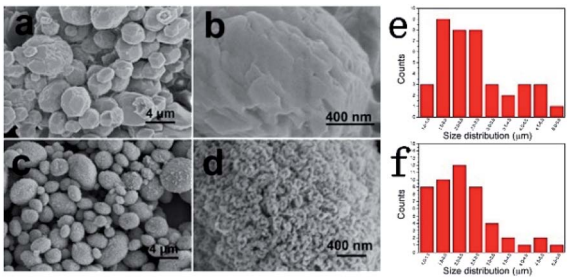

Fig. 3 FE-SEM images of the samples prepared with 0.68 M formic acid (a and b) before heat treatment and (c and d) after heat treatment at 200 °C; (e and f) size distribution of the samples prepared with 0.68 M formic acid before heat treatment and after heat treatment at 200 °C.

indicating that the decomposition rate of manganese formate is very fast.

Fig. 3a and b show FE-SEM images of the sample prepared with 0.68 M formic acid before heat treatment. The ellipsoidal particles are obtained with wide size distribution (see Fig. 3a). The surface of the ellipsoidal particle is rough but no pores are observed (see Fig. 3b). The maximum size, minimum size and mean size of the ellipsoidal particles is 5.20 μm, 1.47 μm and 2.76 μm, respectively. The standard deviation of the sample prepared with 0.68 M formic acid before heat treatment is 1.02 μm. Fig. 3e gives the size distribution of the sample prepared with 0.68 M formic acid before heat treatment. Fig. 3c and d show FE-SEM images of the sample prepared with 0.68 M formic acid after heat treatment at 200 °C. The ellipsoidal microspheres with wide size distribution are prepared (see Fig. 3c). The microspheres are composed of nanoparticles about 20–30 nm and there are a lot of pores in the microspheres, indicating that the microspheres have sponge-like structures (see Fig. 3d). The maximum size, minimum size and mean size of the ellipsoidal microspheres is 5.01 μm, 1.04 μm and 2.40 μm, respectively. The standard deviation of the sample prepared with 0.68 M formic acid after heat treatment is 0.99 μm. Fig. 3f gives the size distribution of the sample prepared with 0.68 M formic acid after heat treatment. EDX pattern of the sample prepared with 0.68 M formic acid after heat treatment at

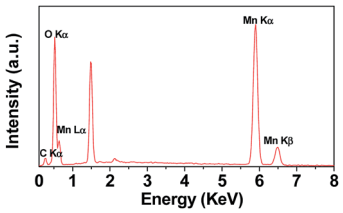

Fig. 4 EDX pattern of the sample prepared with 0.68 M formic acid after heat treatment at 200 °C.

200 °C reveal that the ratio of Mn and O is close to 3 : 4 (see Fig. 4). Comparing with the sample before heat treatment, the sample after heat treatment (Mn_3O_4) exhibits lots of pores (see Fig. 3b and d), while the shape of the microspheres remains almost the same, indicating big collapse or deformation of the structures have been avoided during heat treatment. The size distribution demonstrates a slight change, and the distribution ratio of samples shifts to smaller sizes after heat treatment (see Fig. 3e and f).

FE-SEM images of the sample prepared with 0.68 M formic acid after heat treatment at 350 °C show that the irregular microspheres composed of the particles about 300 nm are obtained, indicating that the high temperature for heat treatment is unfavorable for the formation of the sponge-like structures (see Fig. 5).

Fig. 6 shows TEM images, SAED pattern, HRTEM images and the corresponding FFT patterns of the sample prepared with 0.68 M formic acid after heat treatment at 200 °C. The sponge-like ellipsoidal microspheres are prepared after heat treatment at 200 °C (see Fig. 6a), which is consistent with FE-SEM images (see Fig. 3c and d). The microspheres are composed of nanoparticles about 20–30 nm (see Fig. 6b). According to SAED pattern (see Fig. 6c), the microspheres are assigned to hausmannite. Fig. 6d shows that the pores within sponge-like ellipsoidal microspheres are formed by the aggregation of hausmannite nanocrystals. Fig. 6e shows that two nanocrystals aggregate to form a "neck" between them. According to the corresponding FFT patterns (see Fig. 6f), the two nanocrystals share the (103) facet of hausmannite.

3.2. Effects of formic acid on the morphology and crystal phase of Mn_3O_4

Fig. 7 shows XRD patterns of the samples prepared with various concentration of formic acid. The sample prepared with 1 M

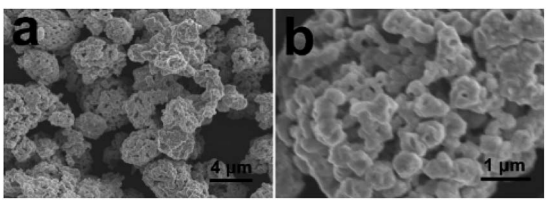

Fig. 5 FE-SEM images of the sample prepared with 0.68 M formic acid after heat treatment at 350 °C.

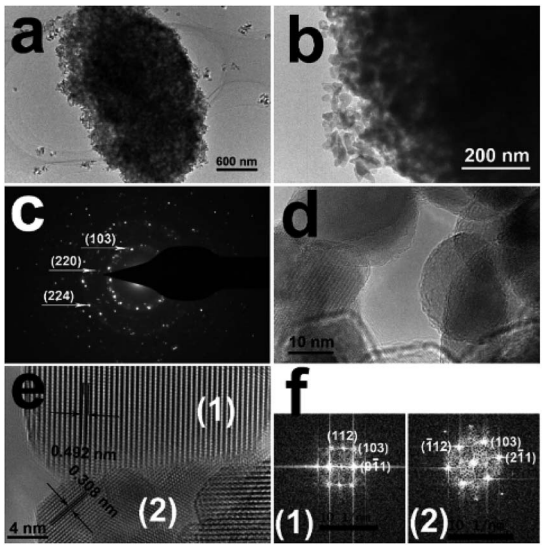

Fig. 6 TEM images (a and b), SAED pattern (c), HRTEM images (d and e) and the corresponding FFT patterns (f) of the sample prepared with 0.68 M formic acid after heat treatment at 200 °C.

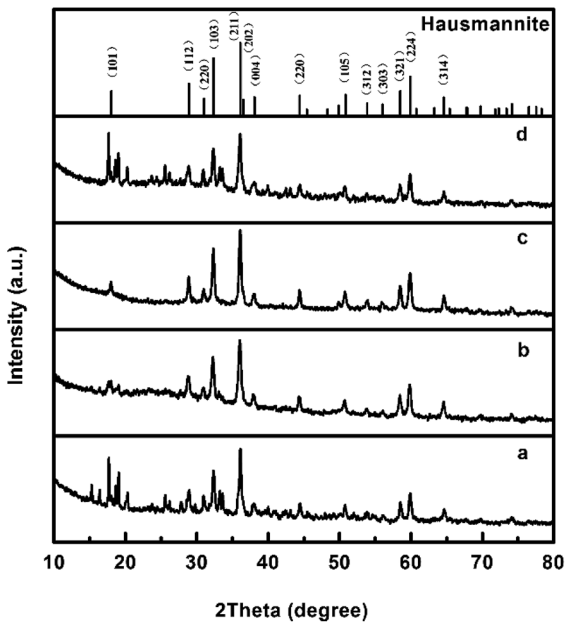

Fig. 7 XRD patterns of the samples prepared with various concentration of formic acid: (a) 0.3 M, (b) 0.42 M, (c) 1 M, (d) 1.28 M.

formic acid are pure hausmannite (see the curve c of Fig. 7), while the samples prepared with 0.3 M, 0.42 M and 1.28 M formic acid contain some unknown phase in addition to hausmannite (see the curve a, b and d of Fig. 7). Fig. 8 shows FE-SEM images of the samples prepared with various concentration of formic acid. The nanoparticles are prepared with 0.3 M and 0.42 M formic acid (see Fig. 8a–d). The irregular sponge-like microspheres are prepared with 1 M formic acid (see Fig. 8e and f). But the sponge-like structures and some objects exhibiting a crystallographic symmetry are prepared with 1.28 M formic

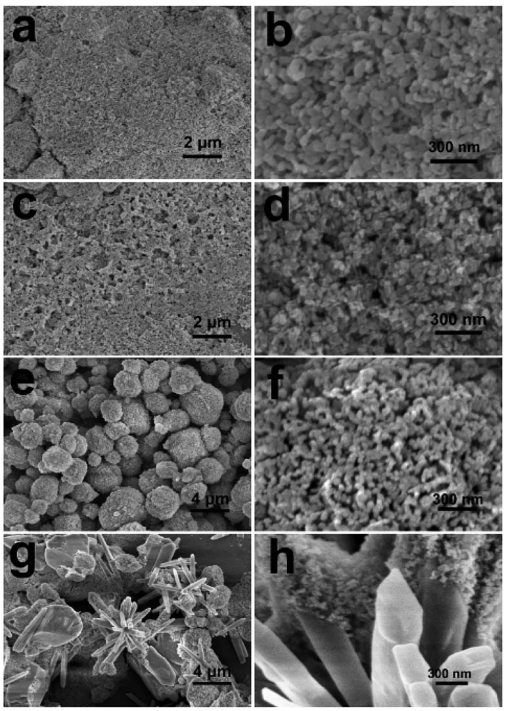

Fig. 8 FE-SEM images of the samples prepared with various concentration of formic acid: (a and b) 0.3 M, (c and d) 0.42 M, (e and f) 1 M, (g and h) 1.28 M.

acid (see Fig. 8g and h). Obviously, the formation of sponge-like hausmannite structures is very sensitive to the concentration of formic acid in such circumstances, and the sponge-like hausmannite structures is obtained with moderate concentration of formic acid.

As revealed in Fig. 3, when the sample is prepared with moderate concentration of formic acid, the morphology of sponge-like Mn_3O_4 structures is mostly retained from the morphology of manganese formate precursor. If the morphology of manganese formate is controlled, the morphology of the sponge-like hausmannite structures might be controlled. The solvothermal process is one of the successful methods to control the growth of manganese formate, which provides an effective pathway to control the morphology of the sponge-like hausmannite structures.

3.3. Effects of solvothermal treatment on the morphology and crystal phase of Mn_3O_4

Fig. 9 shows FE-SEM images of the samples prepared with 0.68 M formic acid for various solvothermal time. When the sample is prepared for 1 h, the spherical sponge-like microspheres are obtained and the small spherical structures begin to appear on the surfaces (see Fig. 9a and b). When the sample is prepared for 6 h, the irregular sponge-like microspheres are obtained and the small spherical structures obviously appear on the surfaces of the microspheres (see Fig. 9c and d). When the sample is prepared for 12 h, the structures exhibiting crystallographic symmetry are obtained (see Fig. 9e), and some of the structures are very large (about 40 μm). As shown in Fig. 9f, the

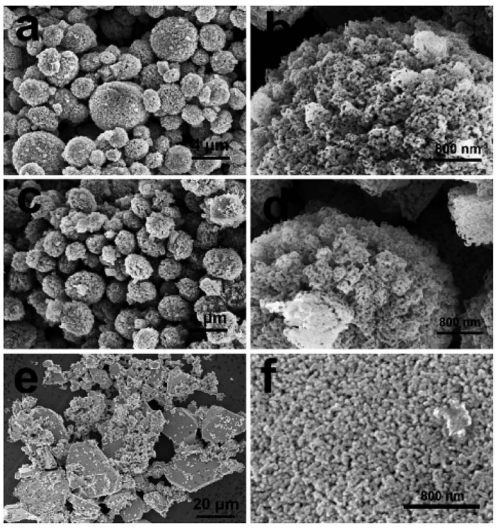

Fig. 9 FE-SEM images of the samples prepared with 0.68 M formic acid for various solvothermal time: (a and b) 1 h, (c and d) 6 h, (e and f) 12 h.

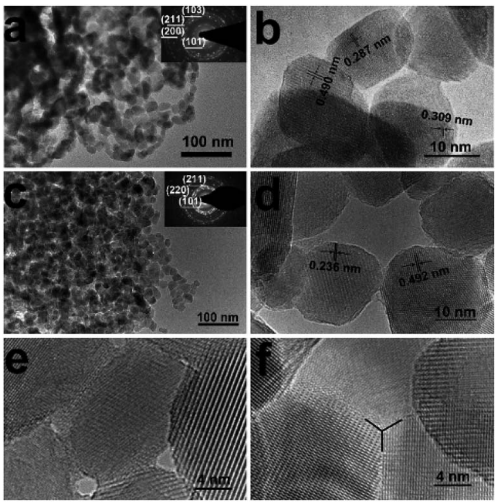

Fig. 11 TEM image (a), SAED pattern (the inset of (a)), HRTEM image (b) of the sample prepared with 0.68 M formic acid under solvothermal treatment for 6 h, TEM image (c) SAED pattern (the inset of (c)), HRTEM images (d–f) of the sample prepared with 0.68 M formic acid under solvothermal treatment for 12 h.

structures are also composed of nanoparticles and pores. The sponge-like structures exhibiting crystallographic symmetry are also prepared for 36 h (see Fig. 10). According to Fig. 9, the morphology of the sponge-like Mn_3O_4 structures is dependent on the solvothermal process.

Fig. 11 shows TEM results of the samples prepared with 0.68 M formic acid under solvothermal treatment for 6 h and 12 h. Fig. 11a shows that the small spherical structures composed of nanoparticles are prepared for 6 h. According to SAED pattern (see the inset of Fig. 11a), the sponge-like structures are confirmed to be hausmannite. Fig. 11b shows that the pores are formed by the aggregation of nanoparticles with high crystallinity. Fig. 11c shows that the sponge-like structures composed of nanoparticles are obtained for 12 h. According to SAED pattern (see the inset of Fig. 11c), the sample are also hausmannite. Fig. 11d shows that the pores about 30 nm are also formed by the aggregation of nanoparticles with high crystallinity. Fig. 11e shows that the pores about 2 nm are formed by sintering of the nanoparticles. Fig. 11f shows that the polycrystalline aggregate is formed by sintering of nanoparticles and the trigeminal grain boundaries are observed within the polycrystalline aggregate. According to Fig. 11, the internal microstructures of the sponge-like structures are independent on the solvothermal process to a certain extent.

3.4. Formation mechanism of sponge-like Mn_3O_4

As described in Section 3.1, sponge-like Mn_3O_4 has similar structure to manganese formate MOF (see Fig. 3). The preparation of sponge-like hausmannite structures (see Fig. 12) involves two steps: the formation of manganese formate and the decomposition of manganese formate. During the first step, due to the low solubility of manganese formate in ethanol, manganese(II) formate is formed by the precipitation reaction between manganese(II) acetate tetrahydrate and formic acid. The sizes of manganese formate precipitates are affected by the concentration of formic acid, and the ellipsoidal manganese formate particles are formed with moderate concentration of formic acid (see Fig. 3a and b). Secondly, the sponge-like Mn_3O_4

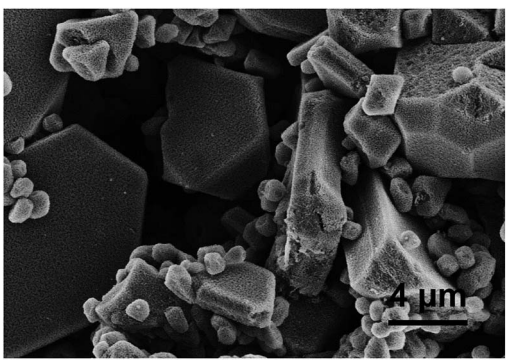

Fig. 10 FE-SEM images of the samples prepared with 0.68 M formic acid under solvothermal treatment for 36 h.

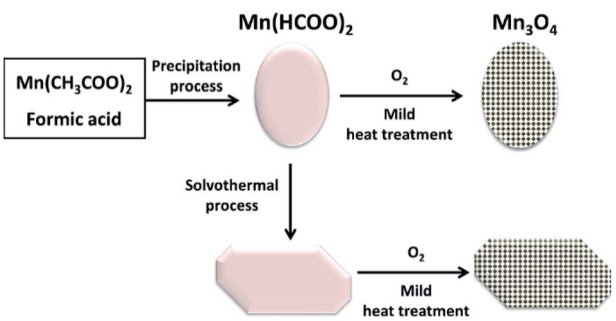

Fig. 12 Scheme illustrating the formation mechanism of sponge-like Mn_3O_4.

microspheres are formed by the thermal decomposition of manganese formate precursor in air. Manganese formate is a kind of MOFs which have abundant channels in the solid. When the heat treatment is operated at 200 °C in air, oxygen can diffuse into the channels because the guest molecules are removed around 180 °C (see Fig. 2). As the heat treatment proceeds, the oxidation of Mn^{2+} may occurs not only on the surfaces of the manganese formate particles but also within the manganese formate particles because of the accessibility of oxygen through the channels (see the ESI†). Moreover, the heat treatment of manganese formate is operated at 200 °C which is much lower than the thermal decomposition temperature of manganese formate (see Fig. 2). Therefore, the thermal decomposition rate of manganese formate particles may be very low, and great structural collapse of the manganese formate particles could be avoided during the decomposition process. On the other hand, the decomposition of manganese formate is an exothermic reaction according to the differential thermal analysis (see Fig. 13). Though the heat treatment is operated at low temperature, during the decomposition process, the heat produced by the exothermic reaction may cause sintering of Mn_3O_4 nanoparticles, leading to the formation of the "neck" among the nanoparticles (see Fig. 6e). Therefore, the structural stability of the sponge-like structures is promoted. Finally, the morphology of sponge-like Mn_3O_4 microspheres can be mostly retained from the morphology of manganese formate precursor. On the other hand, because the decomposition of manganese formate, lots of pores form in the sample (comparing Fig. 3b and d), resulting in increase of surface area.

When the sample is prepared under solvothermal process, the crystal growth of manganese formate occurs *via* Ostwald ripening during the solvothermal process. As the solvothermal process proceeds, the spherical manganese formate particles are gradually formed, leading to the formation of the sponge-like microspheres. As the solvothermal process continues, the large crystals of manganese formate are formed, leading to the formation of the sponge-like structures exhibiting crystallographic symmetry after the heat treatment (see Fig. 9e and f). Therefore, the morphology of the sponge-like Mn_3O_4 structures is dependent on the solvothermal process. The porous Mn_3O_4 structures are created during the heat treatment of manganese formate at 200 °C, and the great structural collapse of manganese formate is also avoid. Therefore, the internal microstructures of the sponge-like structures are independent on the solvothermal process.

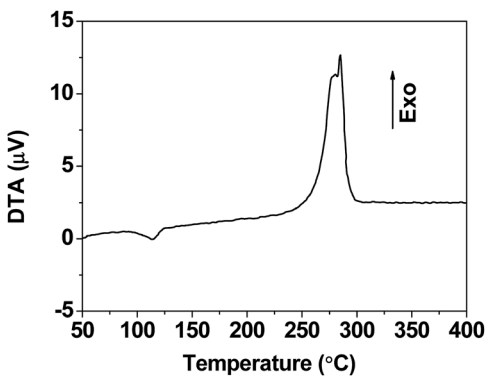

Fig. 13 Differential thermal analysis of manganese formate prepared with 0.68 M formic acid.

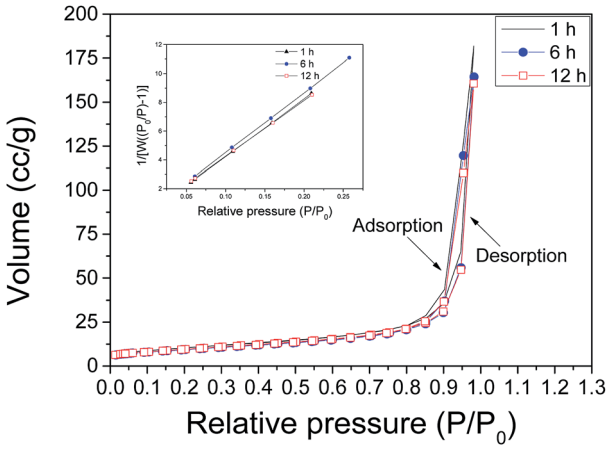

Fig. 14 N_2 adsorption–desorption isotherm of the samples prepared with 0.68 M formic acid for various solvothermal time: 1 h, 6 h and 12 h. The inset plots show BET analysis of corresponding samples.

3.5. N_2 adsorption–desorption analysis

Accordingly, sponge-like Mn_3O_4 structures is obtained at a low temperature of 200 °C *via* a top-down way. Unlike conventional high-temperature calcinated Mn_3O_4, present Mn_3O_4 samples have high specific surface area. Fig. 14 shows the N_2 adsorption–desorption isotherms of the sponge-like Mn_3O_4. A distinct hysteresis in the larger range around 0.85 to 1.0 P/Po suggests the formation of pores originated from the aggregation of hausmannite nanocrystals. The BET surface area of samples prepared for 1 h, 6 h, and 12 h were calculated to be 86.28, 82.87, and 88.55 $m^2\ g^{-1}$, respectively. The sponge-like Mn_3O_4 structures are composed of nanoparticles and pores, which could be responsible for their high surface area. The obtained hierarchical Mn_3O_4 nanostructures would be expected to show superior surface-related properties because of its high specific surface area.

4. Conclusions

The sponge-like Mn_3O_4 structures are prepared by decomposition of manganese formate at 200 °C *via* a facile top-down method. The sponge-like Mn_3O_4 structures prepared with moderate concentration of formic acid are composed of Mn_3O_4 nanocrystals about 20–30 nm and a lot of pores. The morphology of sponge-like Mn_3O_4 structures is mostly retained from the morphology of manganese formate precursor. The morphology of the sponge-like Mn_3O_4 structures is dependent on the solvothermal process before heat treatment. However, the internal microstructures of the sponge-like structures are dependent on the heat treatment process. Large sponge-like structures exhibiting crystallographic symmetry are prepared

under solvothermal treatment for a long time. These hierarchical Mn_3O_4 structures are composed of nanocrystals that form the sponge-like structure with high surface area. These specific textural properties could greatly enhance the chemical properties of the hierarchical sponge-like Mn_3O_4 nanostructures, which make the hierarchical Mn_3O_4 a promising candidate for rechargeable lithium ion batteries, super capacitor and catalysts applications.

Conflicts of interest

There are no conflicts to declare.

Acknowledgements

This research is supported by the Natural Science Foundation of Zhejiang Province of China (Grant No. LY18E020002), the National Natural Science Foundation of China (Grant No. U1809217), the Natural Science Foundation of Zhejiang Province of China (Grant No. LQ16B050002) and Educational Commission of Zhejiang Province of China (Grant No. Y201533271).

References

1 A. Iyer, J. Del-Pilar, C. K. King'ondu, E. Kissel, H. F. Garces, H. Huang, A. M. El-Sawy, P. K. Dutta and S. L. Suib, *J. Phys. Chem. C*, 2012, **116**, 6474–6483.
2 Y. C. Yang, X. Y. Huang, Y. Xiang, S. Chen, L. Guo, S. L. Leng and W. Shi, *J. Alloys Compd.*, 2019, **771**, 335–342.
3 X. S. Lang, F. Ge, K. D. Cai, L. Li, Q. S. Wang and Q. G. Zhang, *J. Alloys Compd.*, 2019, **770**, 451–457.
4 M. H. Alfaruqi, J. Gim, S. Kim, J. Song, P. T. Duong, J. Jo, J. P. Baboo, Z. Xiu, V. Mathew and J. Kim, *Chem.–Eur. J.*, 2016, **22**, 2039–2045.
5 S. Ziller, J. F. von Bulow, S. Dahl and M. Linden, *Dalton Trans.*, 2017, **46**, 4582–4588.
6 B. Ramulu, G. Nagaraju, S. C. Sekhar and J. S. Yu, *J. Alloys Compd.*, 2019, **772**, 925–932.
7 J. Y. Hao, W. P. Li, X. L. Zuo, D. D. Zheng, X. Y. Liang, Y. J. Qiang, B. C. Tan, B. Xiang and X. F. Zou, *J. Mater. Sci.*, 2019, **54**, 625–637.
8 G. R. Xu, J. J. Shi, W. H. Dong, Y. Wen, X. P. Min and A. P. Tang, *J. Alloys Compd.*, 2015, **630**, 266–271.
9 C. Anil and G. Madras, *J. Mol. Catal. A: Chem.*, 2016, **424**, 106–114.
10 G. N. Li, L. Li, Y. Yuan, Y. Y. Yuan, Y. S. Li, W. R. Zhao and J. L. Shi, *RSC Adv.*, 2014, **4**, 35762–35768.
11 H. W. Huang, Q. Yu, X. S. Peng and Z. Z. Ye, *Chem. Commun.*, 2011, **47**, 12831–12833.
12 A. Baykal, Y. Koseoglu and M. Senel, *Cent. Eur. J. Chem.*, 2007, **5**, 169–176.
13 P. T. M. Bui, J. H. Song, Z. Y. Li, M. S. Akhtar and O. B. Yang, *J. Alloys Compd.*, 2017, **694**, 560–567.
14 F. Ji, Y. Men, J. G. Wang, Y. L. Sun, Z. D. Wang, B. Zhao, X. T. Tao and G. J. Xu, *Appl. Catal., B*, 2019, **242**, 227–237.
15 B. G. S. Raj, A. M. Asiri, J. J. Wu and S. Anandan, *J. Alloys Compd.*, 2015, **636**, 234–240.
16 B. Chen, G. H. Rao, S. W. Wang, Y. Lan, L. J. Pan and X. Zhang, *Mater. Lett.*, 2015, **154**, 160–162.
17 L. L. Lan, Q. J. Li, G. R. Gu, H. F. Zhang and B. B. Liu, *J. Alloys Compd.*, 2015, **644**, 430–437.
18 N. John, P. Thomas, K. V. Divya and K. E. Abraham, *Nanotechnology*, 2018, **29**, 10.
19 G. Yanalak, A. Aijabour, E. Aslan, F. Ozel and I. H. Patir, *Int. J. Hydrogen Energy*, 2018, **43**, 17185–17194.
20 A. M. El-Rafei, *Ceram. Int.*, 2015, **41**, 12065–12072.
21 K. A. M. Ahmed, Q. M. Zeng, K. B. Wu and K. X. Huang, *J. Solid State Chem.*, 2010, **183**, 744–751.
22 C. L. Chen, C. L. Dong, G. Chern, K. Kumar, H. J. Lin, C. T. Chen, C. L. Chang and A. Fujimori, *J. Alloys Compd.*, 2014, **614**, 177–181.
23 T. Wang, Q. J. Le, X. L. Guo, M. Huang, X. Y. Liu, F. Dong, J. T. Zhang and Y. X. Zhang, *ACS Sustainable Chem. Eng.*, 2019, **7**, 831–837.
24 C. Y. Zhu, G. Z. Fang, J. Zhou, J. H. Guo, Z. Q. Wang, C. Wang, J. Y. Li, Y. Tang and S. Q. Liang, *J. Mater. Chem. A*, 2018, **6**, 9677–9683.
25 P. Si, X. C. Dong, P. Chen and D. H. Kim, *J. Mater. Chem. B*, 2013, **1**, 110–115.
26 A. Wang, H. Wang, H. Deng, S. Wang, W. Shi, Z. Yi, R. Qiu and K. Yan, *Appl. Catal., B*, 2019, **248**, 298–308.
27 L. Pan, P. Y. Gao, E. Tervoort, A. M. Tartakovsky and M. Niederberger, *J. Mater. Chem. A*, 2018, **6**, 18551–18560.
28 H. J. Peng, G. X. Hao, Z. H. Chu, J. Lin, X. M. Lin and Y. P. Cai, *Cryst. Growth Des.*, 2017, **17**, 5881–5886.
29 P. Losch, T. C. Hoff, J. F. Kolb, C. Bernardon, J. P. Tessonnier and B. Louis, *Catalysts*, 2017, **7**, 19.
30 A. Banerjee, R. Gokhale, S. Bhatnagar, J. Jog, M. Bhardwaj, B. Lefez, B. Hannoyer and S. Ogale, *J. Mater. Chem.*, 2012, **22**, 19694–19699.
31 S. Jung, W. Cho, H. J. Lee and M. Oh, *Angew. Chem., Int. Ed.*, 2009, **48**, 1459–1462.
32 F. Zhang, L. Hao, L. J. Zhang and X. G. Zhang, *Int. J. Electrochem. Sci.*, 2011, **6**, 2943–2954.
33 W. Cho, Y. H. Lee, H. J. Lee and M. Oh, *Chem. Commun.*, 2009, **31**, 4756–4758.
34 B. Liu, H. Shioyama, T. Akita and Q. Xu, *J. Am. Chem. Soc.*, 2008, **130**, 5390–5391.
35 D. N. Dybtsev, H. Chun, S. H. Yoon, D. Kim and K. Kim, *J. Am. Chem. Soc.*, 2004, **126**, 32–33.
36 Z. M. Wang, B. Zhang, H. Fujiwara, H. Kobayashi and M. Kurmoo, *Chem. Commun.*, 2004, **4**, 416–417.

